SAND2018-3431C

Imaging radar performance analysis using product dark regions

Ann Marie Raynal* and Douglas L. Bickel
Sandia National Laboratories, PO Box 5800, Albuquerque, NM, USA 87185-0519

ABSTRACT

Many types of dark regions occur naturally or artificially in Synthetic Aperture Radar (SAR) and Coherent Change Detection (CCD) products. Occluded regions in SAR imagery, known as shadows, are created when incident radar energy is obstructed by a target with height from illuminating resolution cells immediately behind the target in the ground plane. No return areas are also created from objects or terrain that produce little scattering in the direction of the receiver, such as still water or flat plates for monostatic systems. Depending on the size of the dark region, additive and multiplicative noise levels are commonly measured for SAR performance testing. However, techniques for radar performance testing of CCD using dark regions are not common in the literature. While dark regions in SAR imagery also produce dark regions in CCD products, additional dark regions in CCD may further arise from decorrelation of bright regions in SAR imagery due to clutter or terrain that has poor wide-sense stationarity (such as foliage in wind), man-made disturbances of the scene, or unintended artifacts introduced by the radar and image processing. By comparing dark regions in CCD imagery over multiple passes, one can identify unintended decorrelation introduced by poor radar performance rather than phenomenology. This paper addresses select dark region automated measurement techniques for the evaluation of radar performance during SAR and CCD field testing.

Keywords: SAR, Synthetic Aperture Radar, Coherent Change Detection, CCD, Shadows, Radar Performance

1. INTRODUCTION

Verification of proper operations and expected performance of synthetic aperture or coherent change detection imaging radar systems can involve time consuming analysis of an overwhelming number of image products. The need for verification of image products is just as critical for the efficient field testing and debugging of radar systems being prepared for operational deployment, as for monitoring the state of health of an operational system to enable proper maintenance. Furthermore, the front line of individuals responsible for radar system performance evaluation is different for pre-deployment versus operational systems. Both highly specialized radar engineers designing a sensor and highly trained radar operators using a sensor need to be able to identify radar problems efficiently and expediently. To reduce some of the drudgery and skill set requirements (and therefore time and cost) associated with this task, automated algorithms that perform key assessments of radar functionality are not only desirable but necessary. For example, a three-hour flight of Sandia CCD radar systems can easily produce 10,000 image products in stripmap modes and 45,000 images in a video SAR spotlight mode currently. No individual has the time or sustained attention span to look through each product amongst all their other responsibilities, yet identifying and fixing any radar issues as soon as they arise is paramount for successful missions. Consequently, this paper addresses two specific techniques to automate evaluations of proper radar operation and performance in SAR and CCD imaging systems.

Assessments of the utility of radar imagery for operational missions tend to be biased toward the signal energy present in the imagery, rather than the dark regions that constitute a lack of signal energy and a perceived lack of information. However, when identifying and assessing potential radar issues, dark regions do contain valuable information. Noise measurements of dark regions within a SAR image help verify that the expected additive noise and multiplicative noise ratio of a system is within desired requirements or analytical and laboratory measurement values to ultimately maintain adequate signal-to-noise ratios for detection of targets. Depending on the size of the dark region in an image, additive and multiplicative noise levels are commonly measured for SAR performance testing.[1] For additive noise measurements, scenes with a large shadow region with low surrounding clutter are used, whereas small shadow regions with high surrounding clutter usually yield multiplicative noise (though it could be neither additive nor multiplicative). The selection criteria and qualification of an appropriate shadow region for the desired noise measurement type is beyond the scope of this paper and is merely emphasized for the reader to understand that not all shadows are created equal nor suitable for all

* amrayna@sandia.gov; phone 1 505 284-3053; fax 1 505 844-0858; www.sandia.gov/radar

purposes. Other motivations to perform dark region measurements also exist outside the scope of this paper, such as to determine contrast ratios between a target or clutter and noise in SAR imagery. Techniques for radar performance testing of CCD image products (using dark regions or otherwise) are not common in the literature. However, by comparing dark regions in CCD imagery over multiple passes, one can identify unintended decorrelation introduced by poor radar performance rather than phenomenology. Thus, the authors hope to incite similar methodical contributions on radar performance testing for CCD systems with this paper as already exist for SAR.

Many types of dark regions occur naturally or artificially in SAR and CCD products. Occluded regions in SAR imagery, known as shadows, are created when incident radar energy is obstructed by a target with height from illuminating resolution cells immediately behind the target in the ground plane. No return areas (NRAs) are also created from objects or terrain that produce little scattering in the direction of the receiver, such as still water or flat plates for monostatic systems. While dark regions in SAR imagery also produce dark regions in CCD products, additional dark regions in CCD may further arise from decorrelation of bright regions in SAR imagery due to clutter or terrain that has poor wide-sense stationarity (such as foliage in wind), man-made disturbances of the scene, or unintended artifacts introduced by the radar and image processing.

This paper addresses an automated dark region measurement technique for: 1) the evaluation of SAR imagery additive noise performance and, 2) the flagging of radar contributions to poor CCD products and, is organized as follows. Section 2 covers the methodology behind both automated dark region evaluation techniques, while Section 3 details results and discussion regarding the algorithms via an example.

2. METHODOLOGY

The following subsections describe an automated SAR additive noise measurement technique from large shadow regions and a CCD multi-pass technique for identifying and quantifying potential radar problem contributions to decorrelation amidst natural causes for the same.

2.1 Technique for Additive Noise Automated Measurement from Shadows in SAR Imagery

SAR image noise is the root-mean-square (RMS) sum of additive and multiplicative noise.[1] Additive noise is primarily from electronic thermal noise of the radar receiver. It is always present in an image and adds to the scene content. Multiplicative noise is proportional to the average scene intensity. The constant of proportionality, known as the multiplicative noise ratio, is radar hardware driven by analog-to-digital converter quantization, range and azimuth ambiguities, and impulse response sidelobe characteristics. However, coherent integration of sub-resolution terrain surface variations causes pixel-to-pixel fluctuations in the scene intensity of SAR imagery called speckle, which leads to the scene content dependency of multiplicative noise. The total noise over a given area of an image is consequently given by:

$$\sigma_N = \sigma_n + \mathrm{MNR}\overline{\sigma_0},$$

where $\overline{\sigma_0}$ is the average scene clutter reflectivity, MNR is the multiplicative noise ratio, and σ_n is the additive noise. Additive noise is sometimes referred to as the noise equivalent clutter reflectivity (NER) because it analytically corresponds to a terrain that backscatters the same received radar power as the radar's thermal noise power, or in other words, gives a signal-to-noise ratio (SNR) of 1 (i. e. 0 dB).

All SAR noise (and clutter) measurements calculate an area or "distributed target" radar cross-section (RCS) by averaging the intensity values of the RCS-calibrated complex pixels over the given area and normalizing by the ground resolution cell area. An average scene clutter reflectivity measurement is accomplished over the entire image, whereas all noise terms are computed over a NRA. The type of noise that is measurable in a NRA depends on the brightness of the immediately surrounding clutter, size of the NRA portion being measured, and proximity of the NRA to the surrounding clutter sidelobe extent.

Figure 1 summarizes a process for automatically finding an acceptable region within a NRA of a SAR field test image to compute NER. The advantage of this technique over others in the SAR literature[2-3] is that no prior information about the scene content or terrain is necessary to detect the NRA, rather the method is purely data-driven. Additive noise dominates large shadow regions at long ranges and shallow grazing angles. Thus, contriving a field test whereby these conditions are met during collection is highly desirable. We begin by forming a decibel normalized power image of the scene from such a field test collect:

$$\sigma_{image}(x,y) = 10\log_{10}\left[\left(\frac{\cos\psi}{\rho_r\rho_a}\right)|\chi(x,y)C|^2\right] \text{[dB]},$$

where the normalized reflectivity by the *ground* area is given by the azimuth and slant range resolutions ρ_a, ρ_r, respectively, and scene local grazing angle ψ to each image pixel; $\chi(x,y)$ is the complex image value of the *x*th and *y*th range and azimuth image pixel, respectively; and we explicitly include a parameter C for radiometric calibration of the complex image for clarity.

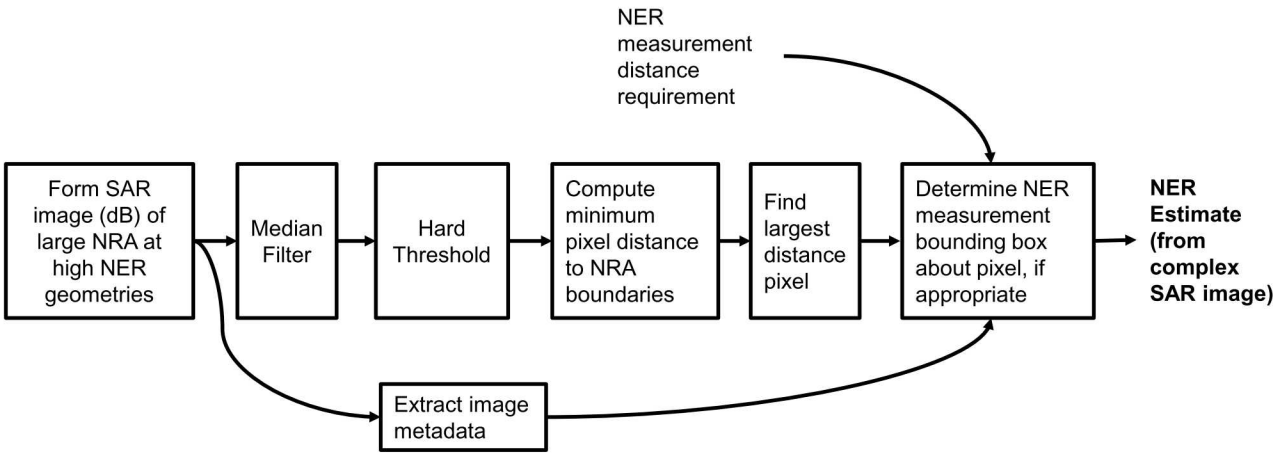

Figure 1. Automated process for finding and measuring additive noise (NER) from a large shadow area

We wish to find the center of the NRA within the scene and gauge that the NRA is of an acceptable size for NER measurements. However, image speckle makes it difficult to proceed; therefore, we next apply some signal processing to reduce its effects. Many filtering and image formation techniques exist to enhance NRAs. The most common and simple methods are mean filtering, resolution coarsening, or median filtering to decrease the speckle variance of the image. Median filtering is the best of the aforementioned methods for edge and shape preservation of NRAs.[4] Furthermore, median filtering the decibel power image, as opposed to the amplitude or intensity image, eliminates the dependence of the speckle variance on the image intensity. Mean filtering followed by median filtering decreases the speckle variance of an image even further, but the added computational cost for large NRAs proves excessive for the designated purpose of NER computations. The median-filtered image by a filter of size [I, J] is given by:

$$p_m(x,y) = F_{[I,J]}\{\sigma_{image}(x,y)\} \text{ [dB]}.$$

A filter size less than [3, 3] m at fine resolution (e.g. 0.1 m) works well per anecdotal evidence. Coarser resolution images might scale this size accordingly, as appropriate. After filtering, the probability distributions of the clutter and noise will tend to be almost bimodal and Gaussian-like.

To detect the NRAs in the filtered image, we use a threshold. While a precise threshold to achieve a given probability of detection or false alarm of NRAs can be analytically computed, the average scene reflectivity of the original complex image in decibels captures a sizeable amount of the clutter distribution (and some noise) in the median-filtered image. Mathematically, this threshold is:

$$\overline{\sigma_0} = 10\log_{10}\left(\frac{1}{N_aN_r\rho_r\rho_a}\sum_x\sum_y \cos\psi\,|\chi(x,y)C|^2\right) \text{ [dB]},$$

where N_a, N_r are the total range and azimuth pixels in the image. Applying the threshold creates a binary image:

$$b(x,y) = (p_m(x,y) > \overline{\sigma_0}).$$

One could also improve upon this threshold and add morphological operations, but these choices again add computational complexity and cost.

After thresholding, we determine the largest suitable NRA in the image. Distance transformation is a common method used in morphological operations to understand the shape and pose of objects.[5] Euclidean distance transformation of the thresholded image helps to gain an understanding of the pixel located in both the largest and most interior part of an NRA

in the image (i. e. the greatest minimum pixel distance from a boundary edge). Mathematically, the distance transformation is given by:

$$d_{Euclid}(x,y) = \begin{cases} \min\limits_{\forall(x_i,y_j)} \left\{ \sqrt{(x_i - x_n)^2 + (y_j - y_m)^2} \right\} & \text{, for } b(x_n, y_m) = 0 \\ 0 & \text{, otherwise} \end{cases},$$

where the binary image and absolute value of its derivatives are one at (x_i, y_j) if the pixel is a boundary edge (i. e. $b(x_i, y_j) = 1$, $\left.\frac{db}{dx}\right|_{x_i} = \pm 1$, and $\left.\frac{db}{dy}\right|_{y_i} = \pm 1$), the binary image is zero at (x_n, y_m) if the pixel is part of a NRA, and the distance function is zero when the pixel is not a part of a NRA. The greatest minimum pixel distance from a boundary edge is then:

$$d_{Euclid}(x_{n_c}, y_{m_c}) = \max_{\forall(x,y)} \{d_{Euclid}(x,y)\}.$$

That pixel, (x_{n_c}, y_{m_c}), should be the center point of the NER measurement area, so long as the NRA size is large enough and far away enough from the boundary edge. We next check that these criteria are met. A reasonable requirement for the NER measurement bounding box is that it both exclude the sidelobe energy extent of an impulse response at the nearest boundary point and encompass the center point for measurement by a pre-established square area. A suggestion is at least 4000 *ground* resolution cells at 0.1-m resolution, or a 40-m^2 area. In other words, the ground distance of the designated center pixel within the NRA to the nearest boundary edge must be greater than the desired (single side of a square) distance requirement. If this requirement is met, then the pixel locations within the bounding box about the designated center point can be used to compute the NER from the complex SAR image. Mathematically, the single side of a square distance requirement is:

$$l_{GndReq} = \sqrt{N_{GndResCellReq}\left(\frac{\rho_r \rho_a}{\cos\psi_c}\right)},$$

where $N_{GndResCellReq} \geq 4000$ as suggested and ψ_c is the grazing angle at scene center for simplicity. Thus, the designated NER measurement area center pixel distance to the boundary edge must meet:

$$d_{Euclid}(x_{n_c}, y_{m_c}) \geq l_{GndReq},$$

or else the bounding box size about the center pixel will violate the exclusion of sidelobe energy from the boundary edges.

If the location of the bounding box center pixel for NER measurement is adequate, the NER can finally then be computed as:

$$\sigma_n = 10\log_{10}\left(\frac{1}{NM\rho_a\rho_r}\sum_{y=x_{n_c}-\frac{N}{2}}^{x_{n_c}+\frac{N}{2}-1}\ \sum_{x=y_{m_c}-\frac{M}{2}}^{y_{m_c}+\frac{M}{2}-1}\cos\psi\,|\chi(x,y)C|^2\right)\ \text{[dB]},$$

where $N = \left\lceil \frac{l_{GndReq}}{\delta_a} \right\rceil$ and $M = \left\lceil \frac{l_{GndReq}\cos\psi_c}{\delta_r} \right\rceil$ are the number of pixels taken for the bounding box in cross-range and ground-range for δ_a, δ_r azimuth and range pixel spacings of the image. We emphasize that the reflectivity averaging should be done as the sum of squares (not square of sums) and with the decibel calculation performed afterwards, lest biases be introduced to the computation by up to 3 dB. Furthermore, the NER measurement should be done on the original complex image, not the median-filtered version which changes the image pixel statistics.

Finally, a check that the measured NER is as expected by comparison to a desired maximum value or within a tolerance of the anticipated analytical value may be applied (i. e. $\sigma_n \leq \sigma_{n\_desired}$ or $\sigma_n \leq \sigma_{n_{analytical}} \pm \sigma_{n_{tolerance}}$ dB). A suggested tolerance value is 3 dB. SAR analytical noise equivalent clutter reflectivity equations, derivations, and typical budgets based on the radar equation are given in the literature[1, 6] to verify field-test radar additive noise performance versus analytical or laboratory radar performance.

2.2 Technique for Examining CCD Image Correlation Performance Using Dark Regions

Decorrelation in a CCD image (i.e. a dark region) is expected from rivers, shadows, and other low-return scene content that also have naturally low signal-to-noise ratios in SAR imagery. Decorrelation of a CCD image can also occur with natural scene content that has high SNR but continual change such as trees due to wind; fields due to growth and irrigation;

terrain due to layover and uncontrolled platform motion; and anthropomorphic activity we want to observe. However, radar problems with repeat pass geometries, autofocus, registration, warping, and so on can manifest as decorrelation in CCD within high SNR SAR image regions as well.

Figure 2 summarizes a process to automatically find images within a CCD repeat pass demonstrating anomalous radar performance. This technique is again, purely data-driven and requires no prior information about the scene content. To cull out radar problems during field testing, we first form co-registered decibel power SAR and CCD image products of a repeat pass:

$$\sigma_{SAR}(x,y) = 10\log_{10}\left[\left(\frac{\cos\psi}{\rho_r\rho_a}\right)|\chi(x,y)C|^2\right]\text{[dB] and } \gamma_{CCD}(x,y) = \frac{\langle \chi_{SARa}\chi_{SARb}{}^{*}\rangle}{\sqrt{\langle|\chi_{SARa}|^2\rangle\langle|\chi_{SARb}|^2\rangle}},$$

where $\langle\ \rangle$ denotes the expectation operator over a sliding window of pixels of the complex SAR image(s) and * denotes the complex conjugate.

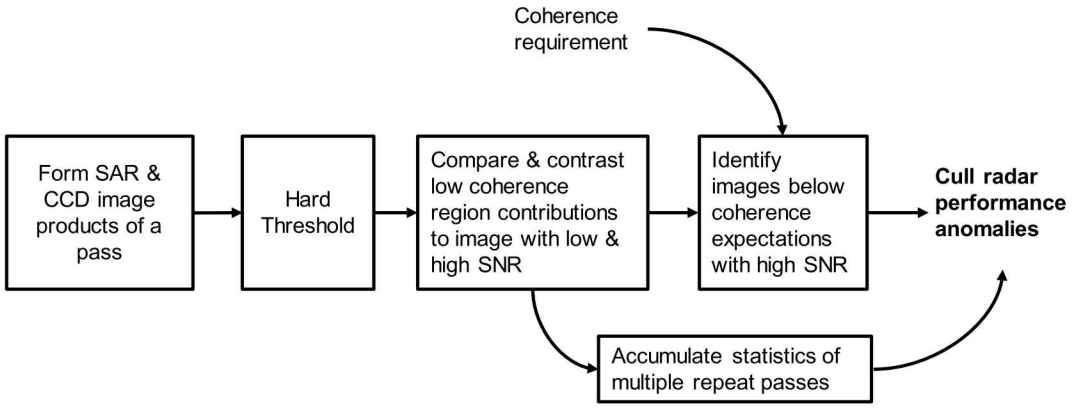

Figure 2. Automated process for finding radar-attributed correlation issues in repeat pass CCD

Next, a hard threshold is applied to the SAR decibel power image and CCD product to find the dark regions in each. A suggested threshold is about -25 dB for SAR fine-resolution, short-range imagery to account for noise but not select too much clutter and 0.6 for CCD products for similar reasons. These thresholds are system-design- or link-budget- dependent and may need to be adjusted as appropriate. Thus, we have binary images:

$$b_{SARa,b}(x,y) = \left(\sigma_{SARa,b}(x,y) < \sigma_{desired}\right) \text{ and } b_{CCDab}(x,y) = \left(\gamma_{CCDab}(x,y) < \gamma_{desired}\right).$$

The pixels of the SAR and CCD products are then contrasted and compared to form the sets of those low in coherence and high in SNR versus those low in both:

$$b_{Low\ SNR,CCD}(x,y) = \left(b_{SARa,b}\ \&\ b_{CCDab}\right) \text{ and } b_{High\ SNR,Low\ CCD}(x,y) = \left(b_{SARa,b} = 0\ \&\ b_{CCDab}\right).$$

We note that median filtering or morphological operations of any binary image can help reduce outlier pixels at the expense of computational cost.

We derive several metrics that are useful at this stage. The first set of metrics are average coherence values for each CCD product in the repeat pass without the low CCD, low/high SNR binary masks applied, i.e.:

$$\overline{\gamma_{CCD,w/o\ LowSNR,CCD}} = \frac{1}{N}\sum \gamma_{CCDab} \notin b_{Low\ SNR,CCD} \text{ and } \overline{\gamma_{CCD,w/o\ High\ SNR,Low\ CCD}} = \frac{1}{N}\sum \gamma_{CCDab} \notin b_{High\ SNR,Low\ CCD},$$

where N is the number of zero-valued pixels in the mask and the image average is computed only over those pixels.

If the average coherence is below some desired value (e.g. 0.6) even after having removed the decorrelated, low SNR pixels of natural scene content from consideration, then there might be a potential radar issue, i.e.:

$$\overline{\gamma_{CCD,w/o\ LowSNR,CCD}} < \overline{\gamma_{CCD,Requirement}} \Longrightarrow phenomenology\ or\ radar\ issue \text{ and}$$

$$\overline{\gamma_{CCD,w/o\ High\ SNR,Low\ CCD}} < \overline{\gamma_{CCD,Requirement}} \Longrightarrow phenomenology\ issue\ only.$$

The second set of metrics is the percentage of pixels of the total image that comprise the dark regions of the CCD whether by low or high SNR, i.e.:

$$Low\ SNR, CCD\ \% = \frac{\sum b_{Low\ SNR,CCD}}{M_{Image}} \text{ x } 100\% \text{ and } \ High\ SNR, Low\ CCD\ \% = \frac{\sum b_{High\ SNR,Low\ CCD}}{M_{Image}} \text{ x } 100\%,$$

where M_{Image} is the total number of pixels in the overall SAR or CCD image.

If the percentage is high for the low coherence, high SNR case contributions to the total image per some threshold and higher than those of the low SNR and coherence case, then there might be a potential radar issue, i.e.:

$$(High\ SNR, Low\ CCD\ \% > Low\ SNR, CCD\ \%)\ \&\ (High\ SNR, Low\ CCD\ \% > Threshold\%) \Longrightarrow phenomenology\ or\ radar\ issue.$$

A conservative threshold percentage is about 20, though the percentage metric is best combined with or rather cued by the average image coherence metric. If the low SNR and coherence case dominates the imagery, then as before, the issue is purely phenomenology-related. (The one caveat is if a low radar transmitter power problem causes the entire image to have low SNR and coherence, but this issue would likely be anomalous compared to other passes over the scene.)

Both sets of metrics can be accumulated for multiple repeat passes to enable a final decision based on consistency of the statistics, which form a coherence map of the scene content natural phenomenology along the collection trajectory. If the low coherence, high SNR patches that are indicating a potential radar issue consistently exhibit poor coherence with high SNR for all passes that is on par with the multi-pass metrics, then natural decorrelation of the scene content is still to blame. Otherwise, there truly is a radar issue for that patch in the pass and the cause should be investigated, i.e.:

$$\left(High\ SNR, Low\ CCD\ \%_{1\ Pass} - \overline{High\ SNR, Low\ CCD\ \%}_{All\ Passes} > Threshold\%\right)\ \&$$

$$\left(\overline{\gamma_{CCD}}_{1\ Pass} < \overline{\gamma_{CCD}}_{All\ Passes} < \overline{\gamma_{CCD,Requirement}}\right) \Longrightarrow radar\ issue\ only.$$

The above decision is best combined with or rather cued by the single-pass criteria.

Once the problem image products are flagged, human intervention is necessary to determine the root cause of the radar issue. Potential sources of error that contribute to decorrelation in CCD products are noted in the literature.[7-9] Note that this technique assumes that temporal baselines of collection areas are kept short enough to be meaningful for such an analysis, since all clutter types completely decorrelate over large time spans and do so at different rates.

3. RESULTS & DISCUSSION

The following subsections show examples of the processing steps and final results of the algorithms described in Section 2, along with some discussion of performance.

3.1 Technique for Additive Noise Automated Measurement from Shadows in SAR Imagery

Figure 3 shows the progression of the algorithm in Section 2.1. Median-filtering, thresholding, Euclidean distance transformation, and the finding of the location (green plus sign) and bounding box (red) of the center region of a large shadow area to automatically measure NER are shown in steps a) through d), respectively, for two different shadow and SAR image scenarios. The shadows were explicitly collected such that they would appear in the far range to measure the worst-case additive noise, computed as -33.6 and -32.2 dB by the algorithm. Note that the scene content, number of shadows, shadow region shapes and sizes, and general location of the large shadow within the image are different, yet still handled appropriately by the algorithm. Note that the left Figure 3c) contains a hole in the distance transformation where there should be shadow caused by imperfections in the median filtering and thresholding of the local speckle in that area. While this case doesn't merit additional mean filtering or morphological operations to fully close the shadow region at the expense of added computational cost, these are possibilities to further deal with unpredictable image speckle for the success of the algorithm. For large shadow areas, as are required for additive noise measurement, we typically find these extra precautions unnecessary.

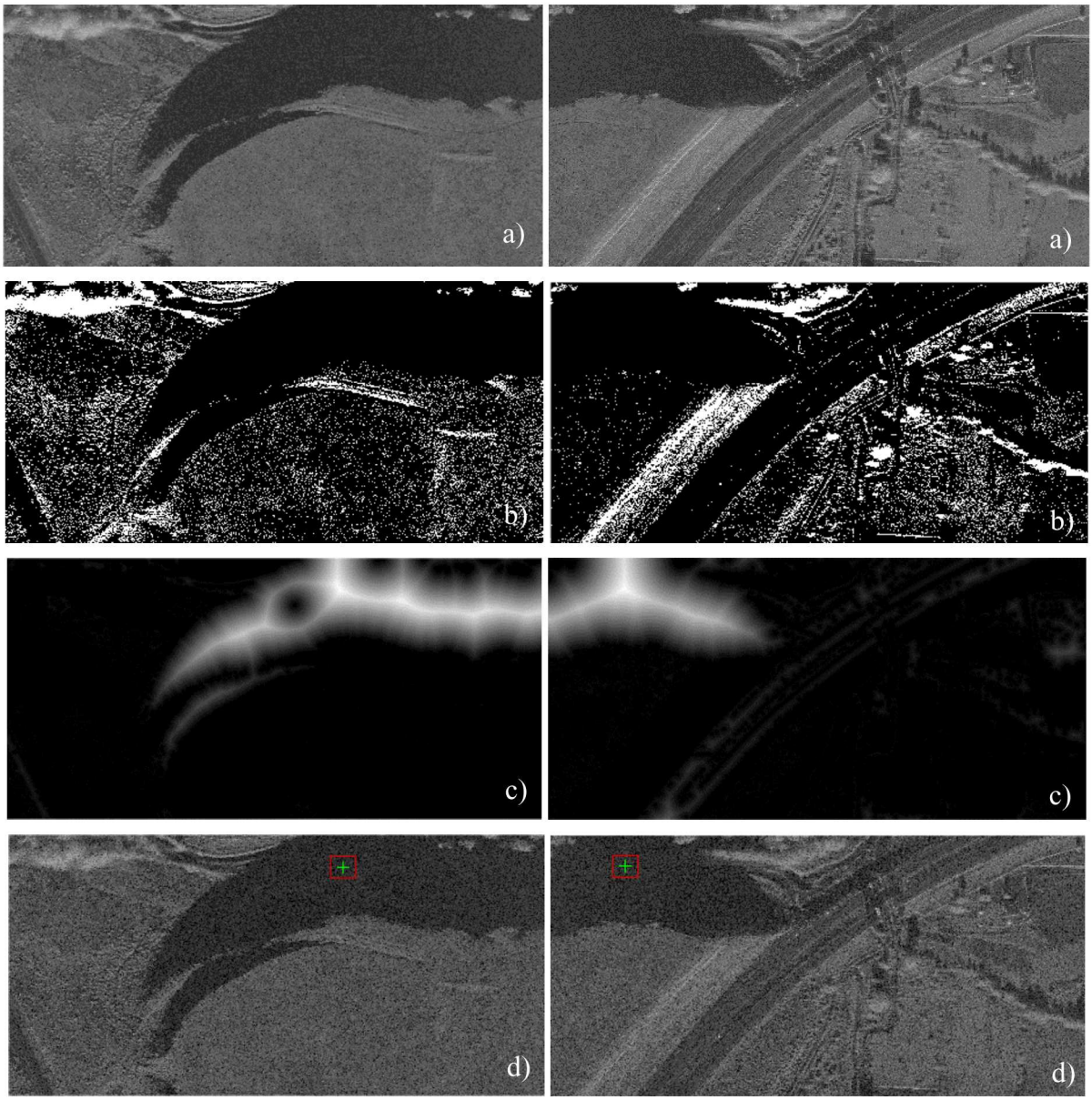

Figure 3. Processing step results for automatically identifying and measuring an additive noise region from a large shadow in a SAR image: a) Median-filtered decibel power image, b) Thresholded binary image by average scene reflectivity, c) Euclidean distance transformation for pixel furthest from shadow boundary, d) Identified center pixel and bounding box for additive noise measurement from original SAR image. Left and right sequences show different shadow and image scenes.

3.2 Technique for Examining CCD Image Correlation Performance Using Dark Regions

Figure 4 through Figure 6 shows the progression of the algorithm in Section 2.2. Figure 4 provides an example of the thresholding and comparison/contrast binary images formed from image pixels with both low coherence and SNR or low coherence with high SNR for a vegetated scene of a river. Figure 5 shows average image coherence and percentage of dark pixel image contributions metrics derived for an entire CCD pass and statistics for multiple repeat passes. The river scene of Figure 4 (Patch 42) is identified as scene with poor coherence but mostly due to low SNR contributions from the river and tree shadows rather than a radar issue, despite not meeting the average coherence desired requirement overall. Patch 11, 44, and 48 on the other hand, have low coherence and high SNR pixel contributions to the overall image dark regions that do not meet a desired average coherence requirement consistently which could indicate a radar problem. Only patch 11, however, is abnormally high in terms of percentage pixel contributions to the dark regions versus the multi-pass average

percentages. Thus Patch 11 is likely a radar issue, whereas Patch 44 and 48 are likely due to natural scene content. Figure 6 confirms these findings with Patch 11 being a phase gradient autofocus point-selection problem with the radar for a fence-line (which is not a point target) amidst uniform clutter (which is also not a point target), rather than the natural decorrelation of fields in Patch 44 and 48. Note that without multiple pass statistics, it would be difficult to disambiguate Patch 44 and 48 as non-radar issues.

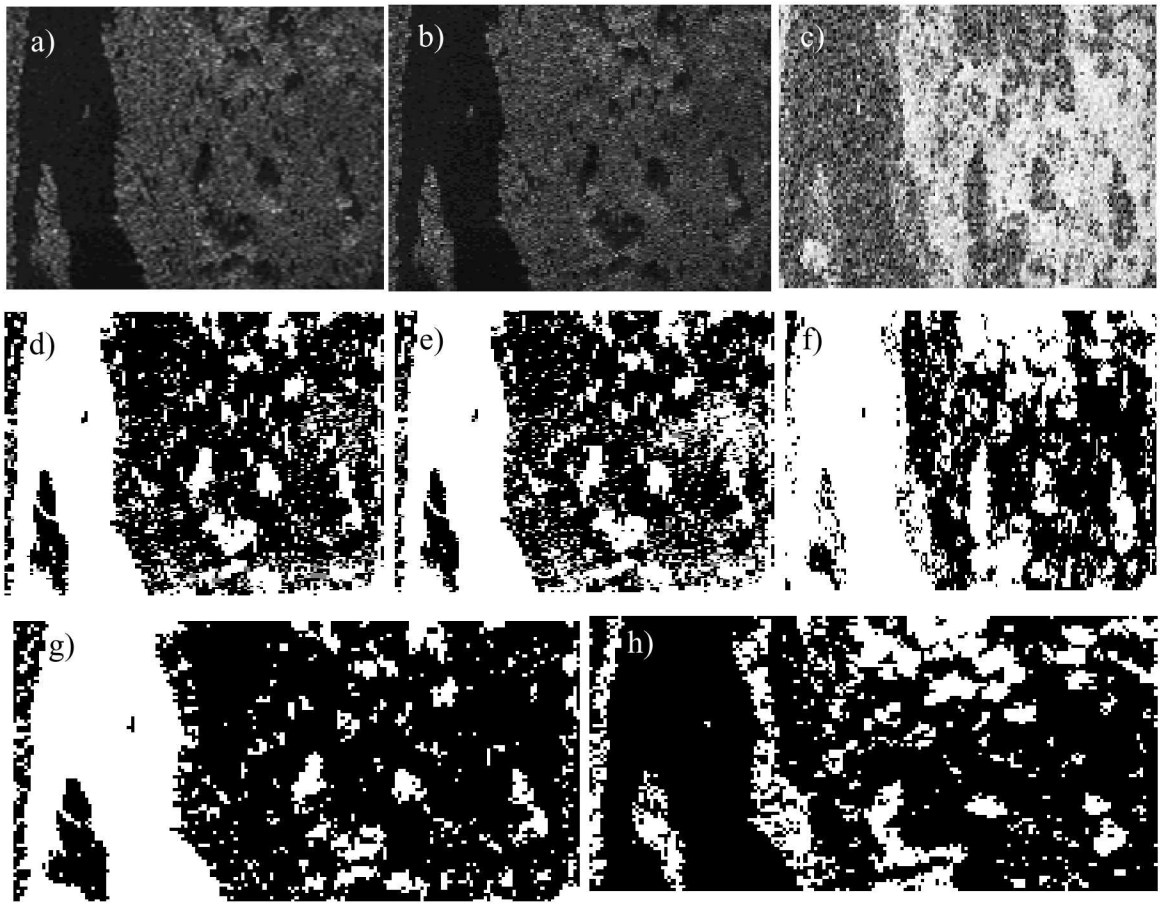

Figure 4. Processing step results for automatically identifying radar problems from a CCD collect: a)-c) Decibel power SAR images and resulting CCD product, d)-f) Corresponding thresholded binary images, g) Comparison binary image of both low coherence and SNR pixels, h) Contrast binary image of low coherence but high SNR pixels.

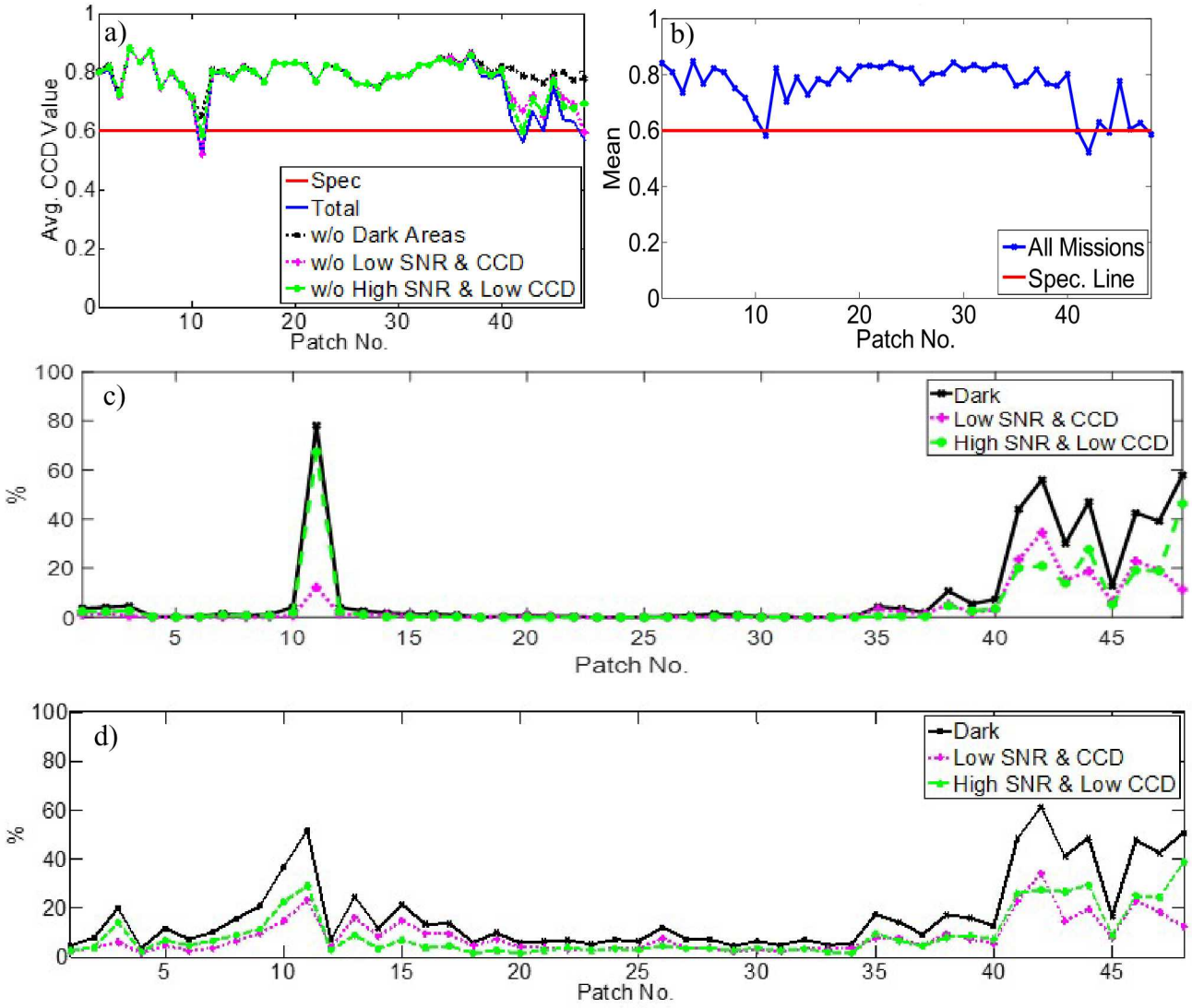

Figure 5. Metrics for automatically identifying radar problems from a CCD collect: a) Average image coherence of dark region contributions to a specific pass relative to a desired requirement, b) Statistical average image coherence of multiple repeat passes relative to a desired requirement, c) Percentage of image pixels accounting for dark region contribution to a specific pass, d) Statistical average percentage of image pixels accounting for dark region contributions in multiple repeat passes. Patch 11, 42, 44, and 48 all indicate severe decorrelation issues per the desired requirement. Only Patch 11 has a larger contribution of dark region pixels with low coherence and high SNR characteristics than the multi-pass average, which is indicative of a radar issue rather than natural scene content.

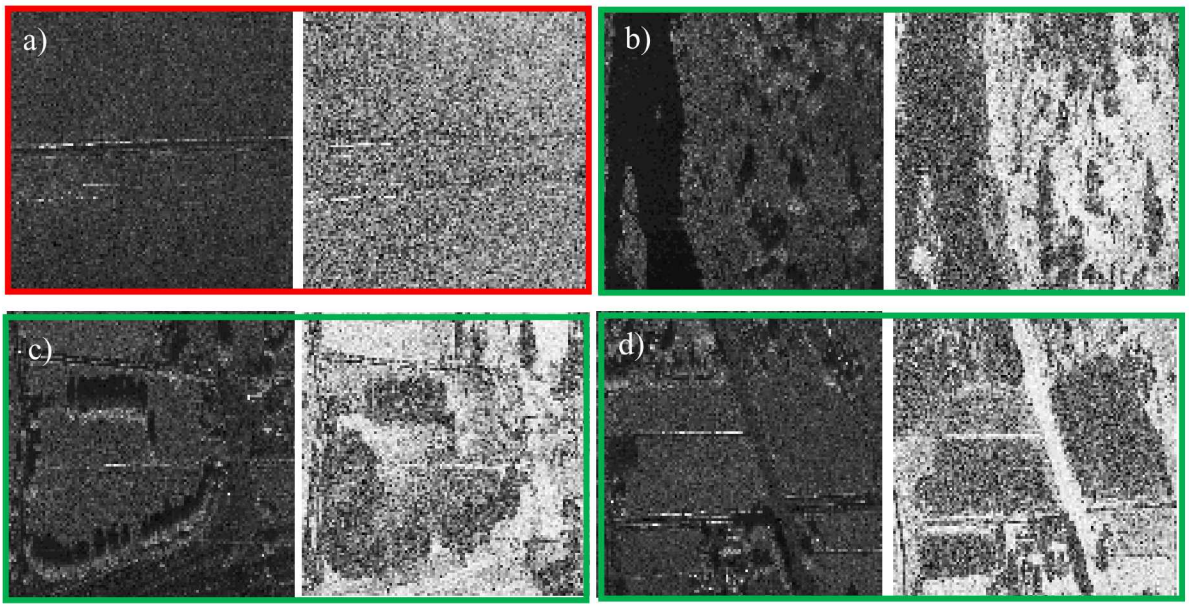

Figure 6. SAR image (left) and CCD product (right) boxed results automatically identifying a radar problem (red) from dark regions in a multi-pass CCD collect versus low decorrelation arising purely due to natural scene content (green): a) Patch 11, identified as a radar issue, b) - d) Patch 42, 44, and 48, identified as non-radar, natural phenomenology issues. (The second SAR image contributing to the CCD product is omitted due to visual similarity to the one shown.)

4. CONCLUSIONS

Verification of proper operations and expected performance of synthetic aperture or coherent change detection imaging radar systems can involve time consuming and costly analysis of many image products by highly skilled engineers or radar operators wishing to understand the state of the radar in the design phases or during operational deployment for maintenance reasons. We have detailed and demonstrated an automated measurement technique for: 1) the evaluation of SAR imagery additive noise performance and, 2) the flagging of radar contributions to poor CCD products to allow for more expedient and efficient analysis of imaging radar system problems. These methods capitalize on the information provided in dark regions of SAR and CCD imagery. While additive and multiplicative noise levels are commonly measured for SAR performance testing in no return areas, the examination of dark region characteristics in CCD imagery over multiple passes to identify unintended decorrelation introduced by poor radar performance rather than phenomenology is not well-known. The SAR algorithm involves a median filter, threshold, and Euclidean distance transformation to detect the innermost location of the largest no return area in an image from which to perform a normalized radar cross-section measurement of the noise. The CCD algorithm involves a thresholding of the SAR and CCD imagery to detect the pixels with low signal-to-noise and coherence that might be attributable to poor radar performance. Statistics within a pass of dark region contributions to an overall average image coherence requirement and total number of pixels within an image as compared to average statistics of the same for several passes indicate inconsistencies within images of a pass caused by radar issues rather than a natural phenomenology coherence map. Both data-driven techniques are shown to work with real-world imagery examples without any prior information about the scene content.

ACKNOWLEDGEMENTS

The imagery used in this report was collected by the Radiant Falcon program, which Sandia executed as a team effort with the Cold Regions Research and Engineering Laboratory (CRREL), U.S. Army Corps of Engineers, Engineer Research and Development Center. The authors wish to thank CRREL for their support.

Sandia National Laboratories is a multi-mission laboratory managed and operated by National Technology and Engineering Solutions of Sandia, LLC, a wholly owned subsidiary of Honeywell International, Inc., for the U. S. Department of Energy's National Nuclear Security Administration under contract DE-NA0003525.

The views expressed in the article do not necessarily represent the views of the U.S. Department of Energy or the United States Government.

REFERENCES

[1] Carrara, W. G. , Goodman, R. S. and Majewski, R. M. , [Spotlight Synthetic Aperture Radar: Signal Processing Algorithms], Artech House, Boston, (1995).

[2] Prasath, V. B. S. and Haddad, O. , "Radar shadow detection in synthetic aperture radar images using digital elevation model and projections," SPIE Journal of Applied Remote Sensing, 8(083628), 1-7 (2014).

[3] Rees, W. G. , "Simple masks for shadowing and highlighting in SAR images," International Journal of Remote Sensing, 21(11), 2145–2152 (2000).

[4] Raynal, A. M. , Miller, J. , Bishop, E. and Horndt, V. , "Shadow probability of detection and false alarm for median-filtered SAR imagery," Sandia National Laboratories Report, 2014(4877), (2014).

[5] Maurer, C. , Rensheng, Q. and Raghavan, V. , "A linear time algorithm for computing exact euclidean distance transforms of binary images in arbitrary dimensions," IEEE Transactions on Pattern Analysis and Machine Intelligence, 25(2), 265-270 (2003).

[6] Doerry, A. W. , "Performance limits for Synthetic Aperture Radar – 2nd Ed.," Sandia National Laboratories Report, 2006(0821), (2006).

[7] Bickel, D. L. , "SAR image effects on coherence and coherence estimation," Sandia National Laboratories Report, 2014(0369), (2014).

[8] Zebker, H. A. and Villasenor, J. , "Decorrelation in interferometric radar echoes", IEEE Transactions On Geoscience and Remote Sensing, 30(5), (1992).

[9] Villasenor, J. and Zebker, H. , "Temporal decorrelation in repeat-pass radar interferometry", Proc. of IGARSS, 2, 941-943 (1992).